

Florian Straube, Frank Schultz, Stefan Weinzierl

On the Effect of Spatial Discretization of Curved Line Source Arrays

Conference paper | Published version

This version is available at <https://doi.org/10.14279/depositonce-8773>



Straube, Florian; Schultz, Frank; Weinzierl, Stefan (2015): On the Effect of Spatial Discretization of Curved Line Source Arrays. In: Fortschritte der Akustik - DAGA 2015: 41. Jahrestagung für Akustik, 16. - 19. März 2015 in Nürnberg. Berlin: Deutsche Gesellschaft für Akustik e.V. pp. 459–462.

Terms of Use

Copyright applies. A non-exclusive, non-transferable and limited right to use is granted. This document is intended solely for personal, non-commercial use.

On the Effect of Spatial Discretization of Curved Line Source Arrays

Florian Straube¹, Frank Schultz², Stefan Weinzierl¹

¹ Audio Communication Group, TU Berlin, 10587, Berlin, Germany, E-mail: florian.straube@tu-berlin.de

² Institute of Communications Engineering, University of Rostock, 18119, Rostock, Germany

Introduction

Line Source Arrays (LSAs) are used for sound reinforcement of large listening areas aiming at sound fields which are as homogenous as possible for the whole audio bandwidth. This contribution presents the analysis of a complex-directivity point source model (CDPS) with respect to spatial discretization as well as tilting effects when employing a curved, uniformly driven LSA setup for a common concert venue. The CDPS-based calculations include far-field radiation patterns of baffled line and circular pistons for the modeling of multi-way cabinets with varying discretization between adjacent drivers. The results are discussed by means of position index plots (PIPs), i. e. sound pressure level spectra for all selected receiver points, and far-field radiation patterns (FRPs) as isobar plots. As expected, it will be shown that sound fields generated by typical LSAs using rather large waveguides are corrupted by spatial aliasing. This can be avoided by applying small individually driven pistons resulting in an increased spatial aliasing frequency.

Spiral Curved LSA

Following [1, 2] generalized formulae for the positioning of the LSA elements were developed based on the spiral curved sources, also known as progressive sources. The main principle of the respective mathematic analysis is that a segment between two points of the spiral is defined by a straight line with the length ΔL , the n -th segment having the tilt angle γ_n with $n = 1, 2, \dots, N$. This is depicted for $\Delta L = \Lambda_{y, \text{LSA}}$ in Fig. 1. In case of the progressive source, the tilt angle of a segment results from the tilt angle of the preceding segment and a preset angle increment, i. e. $\gamma_n = \gamma_{n-1} + (n-1) \Delta\gamma$. The top segment ($n = 1$) can have an initial tilt angle γ_0 equivalent to a tilt offset of the whole spiral. Hence, the tilt angles can be calculated explicitly by

$$\gamma_n = \gamma_0 + \sum_{\eta=1}^{n-1} (\eta - 1) \Delta\gamma = \gamma_0 + \frac{n-1}{2} (n-1) \Delta\gamma. \quad (1)$$

The terminal angle of the spiral then reads

$$\gamma_{\text{final}} = \gamma_N = \gamma_0 + \frac{N-1}{2} (N-1) \Delta\gamma \quad (2)$$

which is equal to the tilt angle of the N -th spiral segment. As prefigured above, the generalized positioning formulae of the top and bottom coordinates can thus be written

as

$$\begin{pmatrix} x_{t,n} \\ y_{t,n} \end{pmatrix} = \begin{pmatrix} x_H \\ y_H \end{pmatrix} - \sum_{\mu=1}^{n-1} \Delta L \begin{pmatrix} \sin \gamma_\mu \\ \cos \gamma_\mu \end{pmatrix}, \quad (3)$$

$$\begin{pmatrix} x_{b,n} \\ y_{b,n} \end{pmatrix} = \begin{pmatrix} x_H \\ y_H \end{pmatrix} - \sum_{\mu=1}^n \Delta L \begin{pmatrix} \sin \gamma_\mu \\ \cos \gamma_\mu \end{pmatrix} \quad (4)$$

using (x_H, y_H) as the initial top position of the first segment, i. e. $(x_{t,1}, y_{t,1}) = (x_H, y_H)$.

LSA Setup

Not only the LSA setup but also the geometry under discussion is schematically depicted in Fig. 1. A total number of $N = 16$ LSA cabinets is used. $\Lambda_{y, \text{LSA}}$ denotes the front grille's height of a single LSA cabinet and is chosen to $\Lambda_{y, \text{LSA}} = 0.372$ m. Note that $\Lambda_{y, \text{LSA}}$ equals the straight line length ΔL from the former section and the front grille top and bottom coordinates of the individual LSA cabinets equal the top (x_t, y_t) and bottom coordinates (x_b, y_b) of the respective spiral segments in this case.

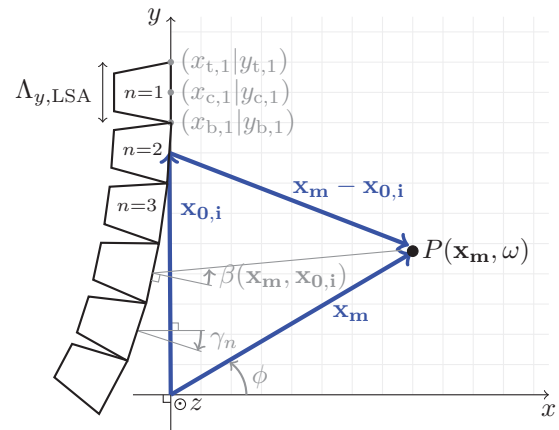


Figure 1: Sketch of the LSA setup under discussion. A total of $N = 16$ LSA cabinets of the height $\Lambda_{y, \text{LSA}} = 0.372$ m are used.

The LSA is built from multi-way cabinets with L_{LF} , L_{MF} and L_{HF} vertically-stacked circular pistons for the low (LF) and mid (MF), as well as line pistons for the high frequency range (HF). Ideal crossover filters with the cut frequencies $f_{\text{LF}, \text{MF}} = 400$ Hz and $f_{\text{MF}, \text{HF}} = 1.5$ kHz are deployed. A modified Active Radiating Factor (ARF) [3, Sec. 3.2], [4, Sec. 3] is used to specify the piston dimensions – i. e. the circular piston radius R and the line piston length Λ_y – related to the fixed distance between adjacent piston centers Δy . The ARF of a line piston

reads [4, (21)], [3, Sec. 3.2]

$$\text{ARF}_{\text{line}} = \alpha = \frac{\Lambda_y}{\Delta y} \quad 0 \leq \alpha \leq 1, \quad (5)$$

whereas the ARF for a circular piston can be written as [4, (26)], [4, (27)]

$$\text{ARF}_{\text{circ}} = \frac{\pi}{4} \alpha^2 = \frac{\pi}{4} \left(\frac{2R}{\Delta y} \right)^2 \quad 0 \leq \alpha \leq 1. \quad (6)$$

α is chosen to 0.82 for both the circular and the line piston – meeting the Wave Front Sculpture Technology (WST) criterion 1 (cf. [3, p. 917]). Considering the characteristics of multi-way cabinets, different piston sensitivities are assumed for the sources in order to obtain realistic sound pressure levels. Two LSA configurations

$$\text{LSA}_1 = \begin{cases} L_{\text{LF}} = 1 \text{ (12 in)} \\ L_{\text{MF}} = 2 \text{ (6 in)} \\ L_{\text{HF}} = 1 \text{ (12 in)} \end{cases} \quad \text{LSA}_2 = \begin{cases} L_{\text{LF}} = 1 \text{ (12 in)} \\ L_{\text{MF}} = 4 \text{ (3 in)} \\ L_{\text{HF}} = 10 \text{ (1.2 in)} \end{cases}$$

with two different sets of the tilt angles γ_n fixed according to the intended audience coverage are examined. The first set is compliant to the WST criterion 5 (cf. [3, p. 929]), whereas the second set does not fulfill this condition for the maximum relative tilt angle (between adjacent LSA cabinets) that amounts to ca. 5.5 deg for the used setup and geometry. In Tab. 1 the chosen tilt angles can be found.

LSA cab.	1	2	3	4	5	6	7	8
$\gamma_{n,1}$ / deg	-3	-1	1	3	5	7	10	12
$\gamma_{n,2}$ / deg	-3	-2	-1	-0.5	1	3	5	7

LSA cab.	9	10	11	12	13	14	15	16
$\gamma_{n,1}$ / deg	15	18	21	24	27	30	34	38
$\gamma_{n,2}$ / deg	8	10	12	15	19	26	33	40

Table 1: Tilt angles of the LSA cabinets for the geometry used (Fig. 1).

With (3) and (4) the front grille center position of the i -th driver of the LSA is given as

$$\mathbf{x}_{0,i} = \begin{pmatrix} x_{0,i} \\ y_{0,i} \end{pmatrix} = \begin{pmatrix} x_{t,n} \\ y_{t,n} \end{pmatrix} + \frac{l-0.5}{L} \begin{pmatrix} x_{b,n} - x_{t,n} \\ y_{b,n} - y_{t,n} \end{pmatrix}, \quad (7)$$

using $l = 1, 2, \dots, L$ and $i = (n-1) \cdot L + l$ for $L = \{L_{\text{LF}}, L_{\text{MF}}, L_{\text{HF}}\}$ with respect to the different frequency bands.

Venue Geometry

An arena with audience and non-audience sections, i. e. zones to be covered and zones to be avoided, is chosen as the concert venue following a practical example presented in [5, Sec. 6.1]. The venue is modeled by a two dimensional slice representation within the xy -plane considering vertical radiation as depicted in Fig. 2, cf. [5–7]. $M = 29\,525$ receiver points with $m = 1, 2, \dots, M$ are taken into account. This corresponds to a distance of 0.005 m between the receiver points ensuring a discretization which approximately equals one fourth of the wave length at 17.2 kHz.

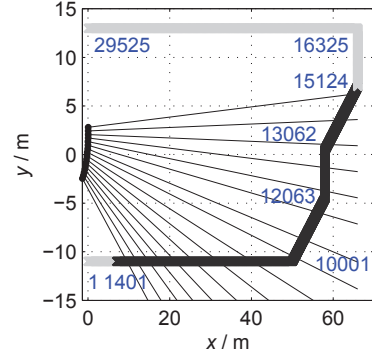


Figure 2: Venue Slice within the xy -plane with audience (black) as well as non-audience/ avoid (gray) zones. The LSA curving is depicted for the first set of tilt angles.

Calculation Model

Based on a complex-directivity point source model of baffled piston far-field radiation patterns, the sound field prediction equation reads [8, (11)], [9, Sec. 1.1]

$$P(\mathbf{x}_m, \omega) = \sum_{i=1}^{LN} D(\mathbf{x}_{0,i}, \omega) \times \underbrace{\frac{e^{-j\frac{\omega}{c}\|\mathbf{x}_m - \mathbf{x}_{0,i}\|_2}}{4\pi\|\mathbf{x}_m - \mathbf{x}_{0,i}\|_2} \frac{\Lambda_{y,\text{LSA}}}{L}}_{G(\mathbf{x}_m, \mathbf{x}_{0,i}, \omega)} \quad (8)$$

using the $e^{+j\omega t}$ time convention. $P(\mathbf{x}_m, \omega)$ denotes the sound pressure spectrum at the receiver position \mathbf{x}_m with $[P(\mathbf{x}_m, \omega)] = 1 \text{ Pa/Hz}$. The complex driving function spectrum $D(\mathbf{x}_{0,i}, \omega)$ with $[D(\mathbf{x}_{0,i}, \omega)] = 1 \text{ Pa/Hz}$ of the i -th source is directly proportional to the source's velocity spectrum. Terming the acoustic transfer function (ATF) from the i -th source to the receiver points, $G(\mathbf{x}_m, \mathbf{x}_{0,i}, \omega)$ is composed of the free-field 3D Green's function (i. e. the spherical monopole) $\frac{e^{-j\frac{\omega}{c}\|\mathbf{x}_m - \mathbf{x}_{0,i}\|_2}}{4\pi\|\mathbf{x}_m - \mathbf{x}_{0,i}\|_2}$, a specific far-field radiation pattern $H_{\text{post}}(\beta(\mathbf{x}_m, \mathbf{x}_{0,i}), \omega)$ and the distance $\Delta y = \Lambda_{y,\text{LSA}}/L$ between adjacent piston centers (discretization step) for L sources per LSA cabinet. The far-field radiation pattern of the baffled circular piston with the radius R and with a constant surface velocity is [10, (26.42)]

$$H_{\text{post,circ}}(\beta, \omega) = \frac{2 J_1\left(\frac{\omega}{c} R \sin \beta\right)}{\frac{\omega}{c} R \sin \beta}, \quad (9)$$

denoting the cylindrical Bessel function of 1st kind of 1st order as $J_1(\cdot)$ [11, (10.2.2)]. Modeling an ideal waveguide for the HF band the far-field radiation pattern of the line piston with the length Λ_y can be written as [10, (26.44)]

$$H_{\text{post,line}}(\beta, \omega) = \frac{\sin\left(\frac{\omega}{c} \frac{\Lambda_y}{2} \sin \beta\right)}{\frac{\omega}{c} \frac{\Lambda_y}{2} \sin \beta}. \quad (10)$$

In line with this modeling, air absorption is neglected, a constant velocity of sound ($c = 343 \text{ m/s}$), infinite, straight baffles and a constant surface velocity are assumed. Note that the sound field prediction equation

(8) correctly synthesizes the collective Fresnel and Fraunhofer region of the whole array if the respective receiver point is located in the far-field of the individual pistons [4]. This does not impose any practical limitations, as the audience is typically located in some meters distance from the individual LSA cabinets. Precise rearward and low-frequency prediction are not feasible by means of this model.

Uniformly Driven LSAs

According to the spatial sampling theorem spatial aliasing can already occur for discretization steps which are larger than half of the wavelength. For the examination of these unwanted effects, the PIPs and the FRPs of the uniformly driven LSAs 1 and 2 are depicted in Fig. 3. A uniformly driven LSA corresponds to an array with sound field adjustment only by geometrical curving and without additional electronic control. Considering the number of individual pistons, the LSA₁ design complies with typical LSAs of the first generation, whereas LSA₂ complies with more recent designs with a larger number of pistons in the MF and HF band.

Discussion

The sound field of the LSA₁ is severely corrupted by spatial aliasing in the whole HF band, whereas the uniformly driven LSA₂ produces considerable aliasing above ca. 9 kHz (theoretical aliasing frequency: 4.61 kHz). The ratio of the audience and non-audience coverage does not turn out to be satisfactory for the LF and the lower frequencies of the MF bands because of the rather non-directed radiation. This ratio is acceptable for the HF band of the LSA₂ up to the frequency the spatial aliasing occurs. Since the effect of the different curving, i. e. the tilt angle sets one and two, can be noticed in the PIPs and FRPs in a very similar way, just the FRPs of the LSA designs with the non-WST5-compliant curving are visualized in the third row of Fig. 3. It can be clearly observed for the high frequencies and in the vertical angle range of ca. -20 deg to -40 deg, as anticipated, that distinct radiation gaps occur for this kind of LSA curving because of the seven-degree relative tilt angles between the last four LSA cabinets.

Conclusion

The presented model is judged to be applicable for the subsequent examination of optimization schemes despite the mentioned assumptions as well as drawbacks and although BEM models and measured LSA data likely provide results that closer match actual LSA sound fields but the latter presumably corrupt the fields so that the influence of optimization effects and inherent imperfections cannot be definitely distinguished. As expected, applying very small individual driven pistons results in an increased spatial aliasing frequency but the reduced power output of smaller pistons must also be taken into account. Additional electronic control is necessary for producing more homogenous sound fields. For a more

profound investigation of the sound fields' characteristics and the radiation behavior, it may be advisable not to restrict the graphical evaluation to PIPs and FRPs but also consider e. g. the sound pressure level distribution in the whole vertical plane in order to gain more comprehensive insight not only into selected extracts but also into the entire LSA near-field as the audience is typically located at the widespread near-field. Furthermore, it may be helpful for the comparison and evaluation of different setups and different driving functions to introduce technical quality measures in the context of LSA design, for example a ratio of the average sound pressure levels of the audience and the non-audience zones, following a more quantitative-based and objective approach of assessment that can make it more convenient to set optimization parameters for electronic control.

References

- [1] Ureda, M.S. (2001): "Line arrays: Theory and applications." In: *Proc. of 110th Audio Eng. Soc. Conv., Amsterdam*, #5304.
- [2] Ureda, M.S. (2004): "Analysis of loudspeaker line arrays." In: *J. Audio Eng. Soc.*, **52**(5):467–495.
- [3] Urban, M.; Heil, C.; Bauman, P. (2003): "Wavefront Sculpture Technology." In: *J. Audio Eng. Soc.*, **51**(10):912–932.
- [4] Schultz, F.; Straube, F.; Spors, S. (2015): "Discussion of the Wavefront Sculpture Technology criteria for straight line arrays." In: *Proc. of the 138th Audio Eng. Soc. Conv., Warsaw*, #9323.
- [5] Thompson, A.; Baird, J.; Webb, B. (2011): "Numerically optimised touring loudspeaker arrays - Practical applications." In: *Proc. of the 131st Audio Eng. Soc. Conv., New York*, #8511.
- [6] Thompson, A. (2009): "Improved methods for controlling touring loudspeaker arrays." In: *Proc. of the 127th Audio Eng. Soc. Conv., New York*, #7828.
- [7] Feistel, S.; Sempf, M.; Köhler, K.; Schmale, H. (2013): "Adapting loudspeaker array radiation to the venue using numerical optimization of FIR filters." In: *Proc. of the 135th Audio Eng. Soc. Conv., New York*, #8937.
- [8] Feistel, S.; Thompson, A.; Ahnert, W. (2009): "Methods and limitations of line source simulation." In: *J. Audio Eng. Soc.*, **57**(6):379–402.
- [9] Meyer, P.; Schwenke, R. (2003): "Comparison of the directional point source model and BEM model for arrayed loudspeakers." In: *Proc. of the Institute of Acoustics*, vol. 25, part 4.
- [10] Skudrzyk, E. (1971): *The Foundations of Acoustics. Basic Mathematics and Basic Acoustics*. New York, Vienna: Springer.
- [11] Olver, F.W.J.; Lozier, D.W.; Boisvert, R.F.; Clark, C.W. (2010): *NIST Handbook of Mathematical Functions*. Cambridge University Press, 1. ed.

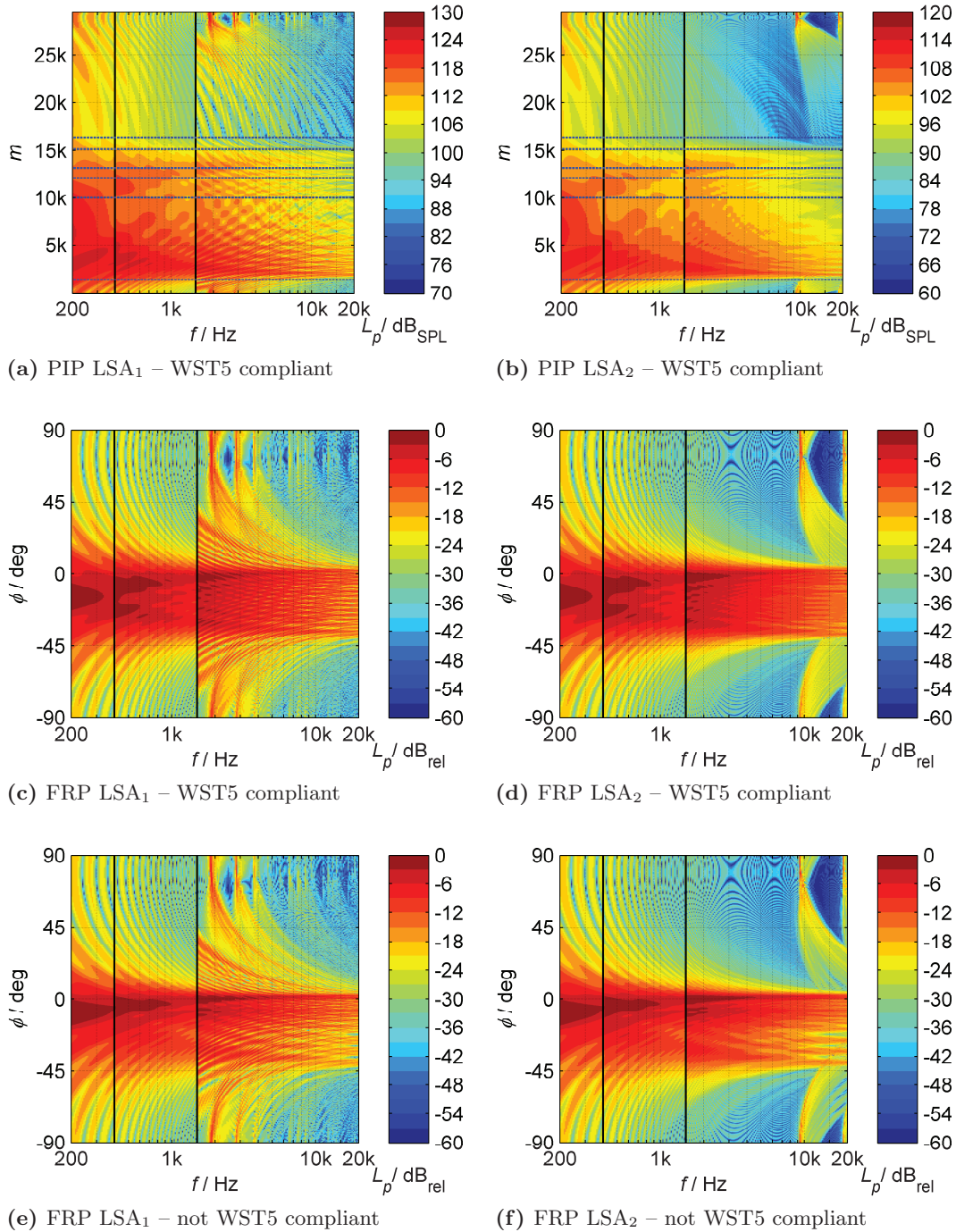


Figure 3: Position Index Plots (PIPs, first row) and Far-Field Radiation Patterns (FRPs, second row) of LSA₁ (left) and LSA₂ (right) – WST5 compliant, i. e. the relative tilt angles (between adjacent LSA cabinets) do not exceed a particular maximum depending on the setup and geometry, in this case: ca. 5.5 deg. Far-Field Radiation Patterns (third row) of LSA₁ (left) and LSA₂ (right) – not WST5 compliant, i. e. at least one of the relative tilt angles exceeds the aforementioned maximum.